Review of Scientific Instruments

Development of a novel type of hybrid non-symmetric flexure hinges

Cite as: Rev. Sci. Instrum. **86**, 085003 (2015); https://doi.org/10.1063/1.4928593
Submitted: 16 May 2015 . Accepted: 03 August 2015 . Published Online: 18 August 2015

Rongqi Wang, Xiaoqin Zhou, Zhiwei Zhu, and Qiang Liu

REVIEW OF SCIENTIFIC INSTRUMENTS **86**, 085003 (2015)

Development of a novel type of hybrid non-symmetric flexure hinges

Rongqi Wang,[1] Xiaoqin Zhou,[1,a)] Zhiwei Zhu,[1,2] and Qiang Liu[1]
[1]*School of Mechanical Science and Engineering, Jilin University, Changchun 130022, China*
[2]*State Key Laboratory of Ultra-Precision Machining Technology, Department of Industrial and Systems Engineering, The Hong Kong Polytechnic University, Kowloon, Hong Kong, China*

(Received 16 May 2015; accepted 3 August 2015; published online 18 August 2015)

A novel type of hybrid non-symmetric flexure hinges (NSFHs) is developed for higher motion precision in this paper, then the finite beam based matrix modeling (FBMM) method is employed to describe elastic deformation behaviors, model compliance matrix, and define non-dimensional precision factors of the hybrid NSFHs. Influences of the dimensional parameters on the dominant compliances and motion accuracies of the NSFHs are analytically investigated based on the FBMM models, while an asymmetry ratio is introduced and its influences on performances of the NSFHs are well revealed. Moreover, making comparisons of the main performances between the proposed NSFHs and symmetric flexure hinges, the obtained results indicate that the hybrid NSFHs can greatly improve the motion accuracy and suppress the adverse inherent motions. Finally, performances of the NSFHs and modeling accuracies are investigated by experimental tests, and making comparison with other flexure hinges. © *2015 AIP Publishing LLC.* [http://dx.doi.org/10.1063/1.4928593]

I. INTRODUCTION

As the extremely important joints in micro electric mechanical systems (MEMSs), various flexure hinges are broadly employed for friction-free and lubrication-free motions with high resolution and high precision. Lots of typical applications can be widely found in many fields, such as the micro-machining systems,[1,2] the micro/nano manipulators,[3,4] and the micro/nano positioning stages.[5,6] So far, many types of flexure hinges with excellent performances have been developed, whose performances depend largely on the various complex-shaped notches. For example, Lobontiu *et al.*[7–12] have developed the generalized models for the corner-filleted flexure hinges, conic-section flexure hinges, circular cross section corner-filleted flexure hinges, and multiple-segment flexure hinges. The closed-form compliance equations and motion accuracies of these hinges were analytically investigated based on the Castigliano's second theorem. Moreover, the generalized models of the conic flexure hinges and elliptical-arc-fillet flexure hinges have been presented through the direct integrations based on the Euler–Bernoulli beam theory.[13–16] Tian *et al.*[17] developed a type of V-shaped fillet flexure hinges for higher performances based on the Castigliano's second theorem, and the power-function-shaped flexure hinges were also proposed with the unit-load method.[18]

In reality, the rotary centers of flexure hinges may deviate from their ideal geometric center, which greatly deteriorate the motion accuracies and block their wider applications. Less center shifts of the flexure hinges are regarded as the common ambitions of many researchers for designing more excellent flexure hinges. As the key metric of motion precision, the precision factors (PFs) were introduced to characterize the motion accuracies of the conic-section flexure hinges, and the related results show that the hyperbolic flexure hinge has the highest motion accuracies.[11,12] Through the reciprocals of the PFs, Tian *et al.*[17] have compared the performances of three types of flexure hinges, namely, the cycloidal, right circle, and V-shaped fillet flexure hinges, and the results indicate the cycloidal flexure hinge has the highest motion accuracy. However, above PFs block fair comparisons due to the negligence of the motion ranges, Li *et al.*[18] introduced a ratio between the PF and the rotation stiffness to more fairly investigate the motion accuracies.

Currently, most existing flexure hinges adopt both transversely and longitudinally symmetric structures, but the bi-symmetric structures greatly restrict their motion accuracies and design feasibilities. Motivated by this, Chen *et al.*[14,19,20] developed two types of hybrid flexure hinges to improve motion accuracies, and the PFs have been introduced to reveal the motion accuracy by the equivalent compliance rotary center.[13,15] Besides, the hybrid hyperbolic corner-filleted flexure hinges were proposed for more excellent performances.[21] However, these hybrid flexure hinges are evenly divided into two equal-length segments with respect to minimum cross sections, while these two segments, namely, the left notch and right notch, will adopt different notch shapes, respectively. Thus, the rotary centers of the hybrid hinges can only indirectly and finitely drift from the geometric midpoint, and this is difficult to directly and arbitrarily adjust the positions of rotary centers for more flexible designs. Given this, a type of exponent-sine-shape flexure hinges (ESFHs) with transversely asymmetric structures have been developed based on the finite beam based matrix modeling (FBMM) method,[22] but the complex-shaped notch will greatly restrict the design flexibility and block broader applications of hinges due to the complex profile and less control variables.

In this paper, a novel type of hybrid non-symmetric flexure hinges (NSFHs) that are transversely asymmetric with respect to their minimum sections is developed to improve the

a)Author to whom correspondence should be addressed. Electronic mail: xqzhou@jlu.edu.cn.

motion accuracy and increase the design flexibility. Performances of two typical hybrid NSFHs are thoroughly investigated by the FBMM method and the experimental tests on practical prototypes.

II. STRUCTURES OF THE HYBRID NSFHs

The 3-D geometric models of the hybrid NSFHs are shown in Fig. 1, where o-xyz are the corresponding Cartesian coordinates; b and t denote the width and the minimum thickness of the flexure hinge; L and c denote the length and the depth of notch, respectively.

As shown in Fig. 1(a), both the left notch and right notch of hinge adopt elliptical notches, called as the elliptical NSFHs, where R_a^L and R_b^L are the major axis and the minor axis of the left elliptical notch; R_a^R and R_b^R denote the similar meaning of the right elliptical notch; and L_1 and L_2 denote the lengths of the left and right notches, respectively. However, when both the major axis of the left and right elliptical notches are particularly equal to their minor axis, namely, $R_a^L = R_b^L$ and $R_a^R = R_b^R$, the elliptical NSFHs evolve to the circular NSFHs, as shown in Fig. 1(b), where R_c^L and R_c^R are the radius of their left and right circular notches. If the left or right notch of the NSFH is circular, while another notch is elliptical, which is a type of hybrid NSFHs, as shown in Fig. 1(c). To investigate influences of the structural asymmetry on the performances of the proposed NSFHs, an asymmetric ratio λ is introduced by

$$\lambda = L_1/L_2. \tag{1}$$

To investigate the proposed NSFHs, the profiles of NSFHs notches are mathematically described by below,

$$\begin{cases} y = -R_b\sqrt{1-\left(\dfrac{x-\lambda L/(1+\lambda)}{R_a}\right)^2} + R_b + \dfrac{t}{2} \\ c = -R_b\sqrt{1-\left(\dfrac{\lambda L/(1+\lambda)}{R_a}\right)^2} + R_b \end{cases}, \tag{2}$$

where, R_a, R_b, and c denote the major axis, minor axis, and depth of the elliptical notch of the NSFH, which can be reasonably chosen based on the notch length L and the asymmetric ratio λ, expressed as follows:

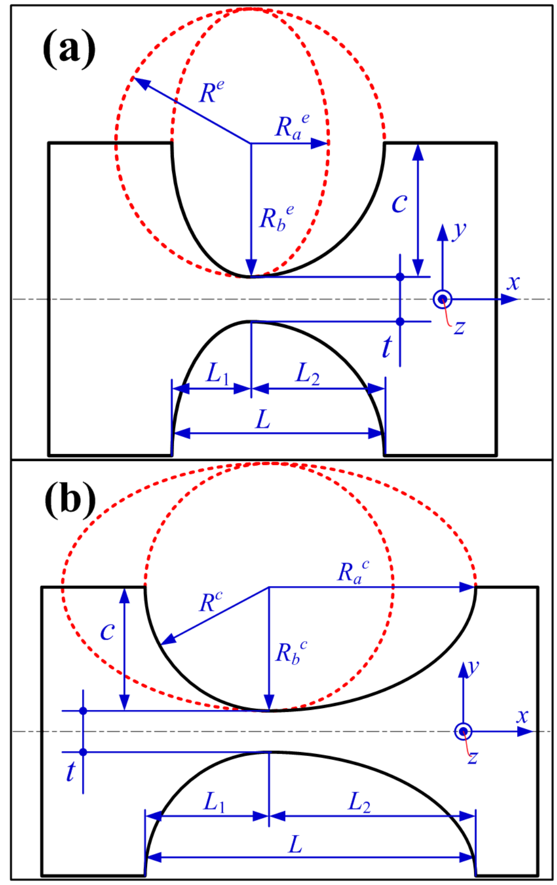

FIG. 2. The geometric features of the hybrid NSFHs. (a) The ENSFHs and (b) the CNSFHs.

$$\begin{cases} R_a = R_a^L, R_b = R_b^L, & 0 \le x \le \lambda L/(1+\lambda) \\ R_a = R_a^R, R_b = R_b^R, & \lambda L/(1+\lambda) < x \le L \end{cases}. \tag{3}$$

Obviously, the notch shapes of the proposed NSFHs are mainly governed by dimensional parameters R_a^L, R_b^L, R_a^R, R_b^R, b, L, c, and λ. To improve the design feasibilities and the availabilities of the NSFHs, the two sorts of hybrid NSFHs are therefore developed as two special cases of the NSFHs, as shown in Fig. 2. The left or right notch of the hinge is circular but another notch is elliptical profile, while the radius

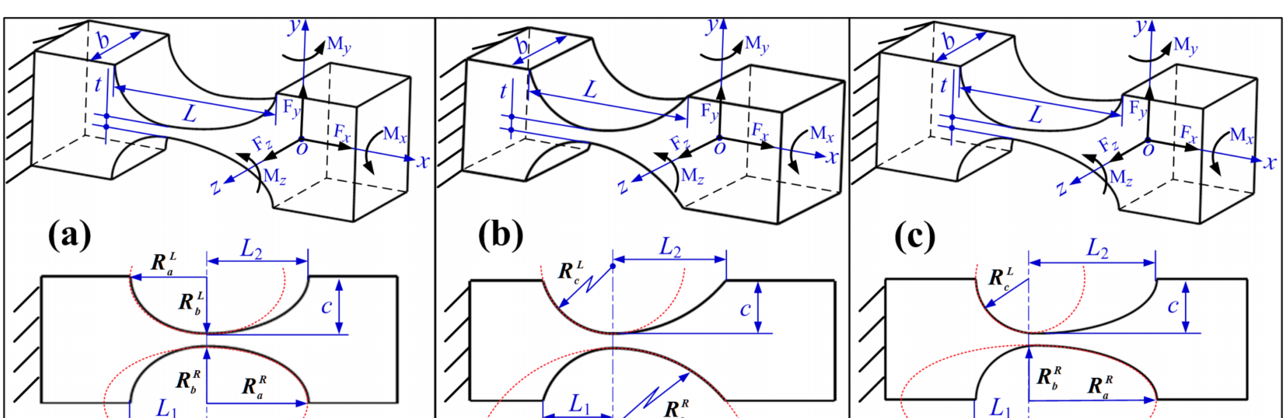

FIG. 1. 3-D geometric model of the non-symmetrical flexure hinge (NSFH). (a) Elliptical NSFH, (b) circular NSFH, and (c) hybrid NSFH.

of circular notch is equal to the major axis or minor axis of the elliptical notch.

As shown in Fig. 2(a), the left notch and right notch of the hybrid NSFH employ the elliptical and circular profiles, respectively, denoted by the ENSFH. Inversely, another sort of hybrid NSFHs (denoted by the CNSFHs) adopts circular and elliptical shapes as their left and right notches, respectively, as illustrated in Fig. 2(b). To reveal dependences of the notch profiles to asymmetric ratio λ of the two types of hybrid NSFHs, different notch curves in terms of variable λ are shown in Fig. 3. When λ ranges from 1/3 to 4/3, notch profiles of the two hybrid NSFHs are shown in Figs. 3(a) and 3(b), respectively. Next, the remainder of this paper will mainly concentrate on investigating the two types of hybrid NSFHs in detail.

III. COMPLIANCE AND MOTION ACCURACY MODELING

To more simply but effectively describe the elastic deformation behaviors of flexure hinges, a novel FBMM method proposed by authors before will be introduced to avoid laborious integral operations,[22,23] and the followings are the modeling processes of the hybrid NSFHs.

A. Compliance modeling with the FBMM method

Based on Hooke's law, the relationship is derived as follows:

$$\mathbf{\Delta} = \mathbf{C}\,\mathbf{F}, \tag{4}$$

where, $\mathbf{F}$ and $\mathbf{\Delta}$ are, respectively, defined as the unit load vector and corresponding deformation vector and $\mathbf{C}$ denotes the compliance matrix. This paper will concentrate on the compliance modeling with the FBMM method that assumes the flexure hinge to be a combination of finite Euler-Bernoulli micro-beams with serial connections, so $\mathbf{C}$ can be mathematically described by[22,23]

$$\mathbf{C} = \sum_{i=1}^{N} \mathbf{T}_i\mathbf{C}_i\mathbf{T}_i^{\mathbf{T}}, \quad \mathbf{T}_i = \begin{bmatrix} \mathbf{R}_i & \mathbf{S}_i(\mathbf{r}_i)\,\mathbf{R}_i \\ \mathbf{0} & \mathbf{R}_i \end{bmatrix}, \tag{5}$$

where $\mathbf{C}_i$ denotes the compliance matrix of the ith single micro-beam in its local coordinate.[22,23] $\mathbf{T}_i$ denotes the compliance transformation matrix (CTM) the ith local coordinate with respect to the global coordinate. N is the total number of the divided micro-beams. $\mathbf{R}_i$ denotes the rotation matrix of the local coordinate with respect to the global coordinate. $\mathbf{r}_i$ represents the position vector of the local coordinate in the global coordinate. $\mathbf{S}_i(\mathbf{r}_i)$ denotes the skew-symmetric operator for the vector $\mathbf{r}_i$,

$$\mathbf{S}_i(\mathbf{r}_i) = \begin{bmatrix} 0 & -z_i & y_i \\ z_i & 0 & -x_i \\ -y_i & x_i & 0 \end{bmatrix}, \qquad \mathbf{r}_i = \begin{bmatrix} x_i \\ y_i \\ z_i \end{bmatrix}^{\mathbf{T}}. \tag{6}$$

In Eq. (7), E and G are the modulus of elasticity and the modulus of rigidity. dx and b denote the length and width of the single micro-beam. h_i represents the height of the ith divided micro-beam, which can be obtained by the formula $h(x) = 2y(x)$, and k denotes the shape factor of the torsional deformation.[24]

$$\mathbf{C}_i = \begin{bmatrix} \frac{dx}{Ebh_i} & 0 & 0 & 0 & 0 & 0 \\ 0 & \frac{4dx^3}{Ebh_i^3} + \frac{dx}{Gbh_i} & 0 & 0 & 0 & \frac{6dx^2}{Ebh_i^3} \\ 0 & 0 & \frac{4dx^3}{Eb^3h_i} + \frac{dx}{Gbh_i} & 0 & -\frac{6dx^2}{Eb^3h_i} & 0 \\ 0 & 0 & 0 & \frac{dx}{Gkbh_i^3} & 0 & 0 \\ 0 & 0 & -\frac{6dx^2}{Eb^3h_i} & 0 & \frac{12dx}{Eb^3h_i} & 0 \\ 0 & \frac{6dx^2}{Ebh_i^3} & 0 & 0 & 0 & \frac{12dx}{Ebh_i^3} \end{bmatrix}. \tag{7}$$

To verify the established FBMM model, the finite element analysis (FEA) on three series of hybrid NSFHs with different dimensional parameters, which are listed in Table I, is conducted by the widely adopted ANSYS Workbench. The chosen material (spring steel) with the Young's modulus and Poisson's ratio is $E = 2 \times 10^{11}$ Pa and $\mu = 0.288$. The in-planar compliances obtained by the FEA and the FBMM method are presented in Table II, the relative errors (denoted by e) between the FEA results (denoted by F) and analytical results (denoted by A) are calculated through taking the FEA results as the ideal values. As shown in Table II, all the relative errors e are less than 5%, which indicates a good agreement between the FEA and analytical results, well demonstrating the established FBMM models of the NSFHs can effectively characterize their elastic deformation behaviors.

In addition, it is also very important to evaluate the maximum stresses of hinges from the displacement fields

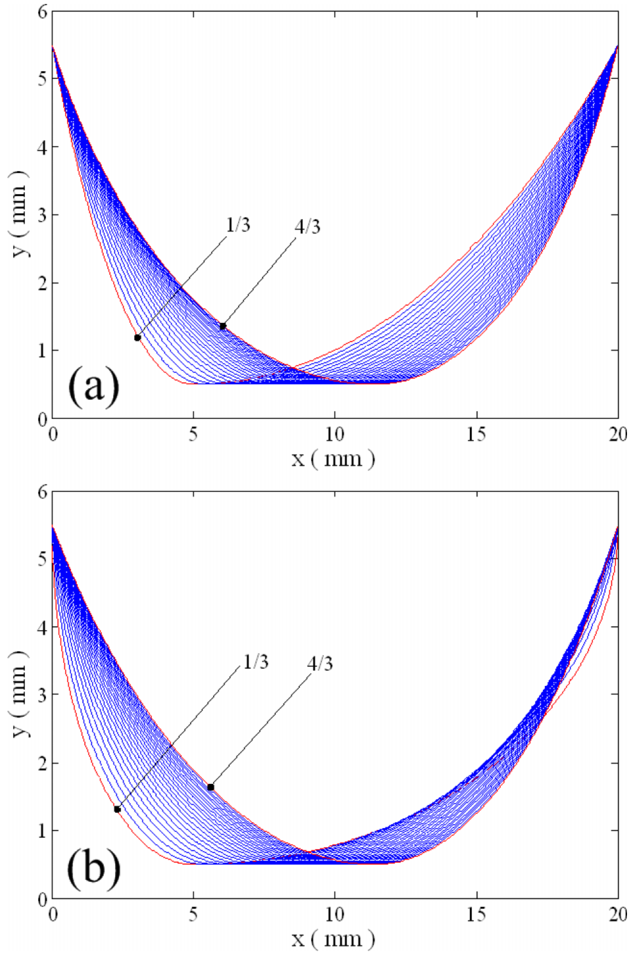

FIG. 3. Profiles of the hybrid NSFHs in terms of the asymmetric ratio λ. (a) The ENSFHs and (b) the CNSFHs.

When only the in-plane bending and axial effects are considered, the maximum stress on the cross section with minimum thickness can be expressed[12]

$$\sigma_{\max} = 6\frac{k_b}{bt^2}\left[(K_{6,6} + L_2 \cdot K_{6,2})\,\theta_z + (K_{6,2} + L_2 \cdot K_{2,2})y\right] + \frac{k_a}{bt}K_{1,1}x, \qquad (8)$$

where $K_{6,6}$, $K_{6,2}$, $K_{2,2}$, and $K_{1,1}$ are the stiffnesses in the corresponding directions, which are the reciprocals of the compliances $C_{6,6}$, $C_{6,2}$, $C_{2,2}$, and $C_{1,1}$, respectively; the stress concentration factors in bending k_b and axial k_a are specified in Ref. 25. This formula is also verified by FEA method in Table II, and the maximum displacement vectors x and y are both set as 10 μm. The relative errors between the analytical and FEA results are less than 5%, which indicates the maximum stress formula is accurate for describing the maximum stress of the proposed hybrid NSFHs from the displacement fields.

B. Motion accuracy modeling and verification

In practice, the rotary centers of flexure hinges may adversely drift and cause undesirable motion deviations due to their elastic deformations. To describe the motion accuracies of the two hybrid NSFHs, the planar motion deviations of the rotary centers in the x and y directions are also calculated as the motion precisions by the above FBMM method.[22,23] The motion accuracies are generally regarded as the very significant performance criteria for designing the flexure hinges.

The schematic of hybrid NSFH with external loads is shown in Fig. 4, where O_1 denotes the rotary center; F_x, F_y, and M_z are the external loads exerted on the free end; F_{1x} and F_{1y} are the equivalent forces on the rotary center induced by external forces F_x and F_y; and M_{1z} denote the total equivalent moments at rotary centers caused by external forces F_y and moments M_z. The equivalent generalized forces on the center O_1 can be expressed as follows:

$$\mathbf{F}_G = \begin{bmatrix} F_{1x} & F_{1y} & M_{1z} \end{bmatrix}^{\mathrm{T}} = \begin{bmatrix} F_x & F_y & M_z + F_y \cdot L_r \end{bmatrix}^{\mathrm{T}}, \qquad (9)$$

where L_r denotes the distance of rotary center to the free end. The rotary center of the NSFH will diverge from the midpoint of the minimum cross section; thus, L_r can be determined by:[26]

$$L_r = \frac{\delta y}{\delta\theta_z} = \frac{\delta y/M_z}{\delta\theta_z/M_z} = \frac{C_{y,M}}{C_{\theta,M}}. \qquad (10)$$

$\Delta_1 = [e_{x1}\, e_{y1}]^{\mathrm{T}}$ will be defined as the drift components of the rotary centers when external loads are exerted on the free ends of the hinges, namely, the translational drifts along the x_1-axis and y_1-axis. Based on the Hooke's law, the relationship between the drift components Δ_1 and equivalent external loads F_G can be expressed by

$$\Delta_1 = \Theta \cdot \mathrm{F}_G = \begin{bmatrix} e_{x1}/F_{1x} & 0 & 0 \\ 0 & e_{y1}/F_{1y} & e_{y1}/M_z \end{bmatrix} \cdot \begin{bmatrix} F_{1x} \\ F_{1y} \\ M_{1z} \end{bmatrix}, \qquad (11)$$

$$\mathbf{\Theta} = \sum_{i=1}^{(L-L_r)/dx} \mathbf{T}_{1i}\mathbf{C}_i\mathbf{T}_{1i}^{\mathrm{T}}, \qquad T_{1i} = \begin{bmatrix} 1 & 0 & y_i \\ 0 & 1 & -x_i \\ 0 & 0 & 1 \end{bmatrix}, \qquad (12)$$

where, Θ denotes the planar compliance matrix at the rotary center,[22] each element of Θ has been defined as the PF.[14,15] Similar to the compliance matrix C, $\mathbf{C}_i$ is the compliance matrix of the ith single unit-beam in its local coordinate and $\mathbf{T}_{1i}$ is the planar compliance transformation matrix.[5]

The defined PF[18] was proposed as an absolute physical parameter to describe the undesired drifts of rotary centers with considering motion range of the hinge, but the PFs have non-uniform dimensions. In authors' previous studies, the non-dimensional precision factors (NDPFs) are proposed to be the key performance criteria,[22] which means the ratios

TABLE I. Parameters of the proposed hybrid non-symmetrical flexure hinges.

Example	R_a^L (mm)	R_b^L (mm)	R_a^R (mm)	R_b^R (mm)	L (mm)	t (mm)	c (mm)	b (mm)
1	6	6	12	6	18	1.2	6	12
2	6	15	15	15	18	1.2	6	12
3	9.7	9.7	9.7	9.7	18	1.2	6	12

TABLE II. Comparisons between FEA and analytical results (in SI unit).

	$\delta x/F_x(\times 10^{-9}\,\mathrm{m/N})$			$\delta y/F_y(\times 10^{-6}\,\mathrm{m/N})$			$\delta y/M_z(\times 10^{-4}\,1/\mathrm{N})$			$\delta\theta_z/M_z(\times 10^{-4}\,1/\mathrm{N})$			$\sigma_{\max}$ (MPa)		
	A	F	e(%)	A	F	e (%)	A	F	e (%)	A	F	e (%)	A	F	e (%)
1	2.98	3.09	3.6	1.61	1.58	1.9	1.41	1.38	2.2	1.29	1.27	1.6	274.3	279.3	1.9
2	2.57	2.64	2.7	1.33	1.32	0.8	1.15	1.14	0.9	1.04	1.03	1.0	243.4	234.4	3.8
3	2.69	2.82	4.6	0.944	0.923	2.3	0.999	0.974	2.6	1.11	1.08	2.8	246.4	235.8	4.5

of the deviations of the rotary centers to the generalized displacements of the free end under same loads, as expressed in following:

$$\boldsymbol{\beta} = \begin{bmatrix} \beta_1 \\ \beta_2 \\ \beta_3 \end{bmatrix} = \begin{bmatrix} e_{x1}/\delta x \\ e_{y1}/\delta y \\ e_{y1}/\delta y \end{bmatrix} = \begin{bmatrix} \frac{e_{x1}}{F_x} & \frac{e_{y1}}{F_y} & \frac{e_{y1}}{M_z} \\ \frac{\delta x}{F_x} & \frac{\delta y}{F_y} & \frac{\delta y}{M_z} \end{bmatrix}^{\mathrm{T}}. \tag{13}$$

Similar to verify the planar compliances of hinges, the precision factors are also calculated by both the FEA and FBMM methods, as listed in Table III. Then, the FEA results will be regarded as the accurate values for further calculating the relative errors with the FBMM results. As listed in Table III, the maximum relative error is about 10%, which shows the FEA results can well agree with the FBMM results. The fine results demonstrate that the NDPF modeling method is very effective and can well describe the motion accuracies of the hybrid NSFHs.

IV. PERFORMANCE ANALYSIS AND DISCUSSION

A. Influence of the dimensional parameters on the planar compliances

In view of the planar motions of the hinges are more dominant than the motions in the other directions, thus influences of the dimensional parameters on these planar compliances are analytically investigated based on the FBMM method. As shown in Fig. 2, five dimensional parameters, marked by t, b, c, L, and λ, co-determine the notch shapes of the designed hinges, which are therefore employed for describing the elastic deformation behavior of the hybrid NSFHs. Obviously, parameters c, L, and λ determine the notch shapes of the hinges, while variables b and t determine the structure features of the NSFHs. Thus, this research will focus on the influences of former three size parameters on the planar compliances, namely, $\delta x/F_x$, $\delta y/F_y$, $\delta y/M_z$, and $\delta\theta_z/M_z$. To investigate influences of the parameters L and c, variables b, t, and λ are first assumed to be 10 mm, 1 mm, and 0.5, while parameters L and c range from 10 mm to 20 mm and 3 mm to 8 mm,

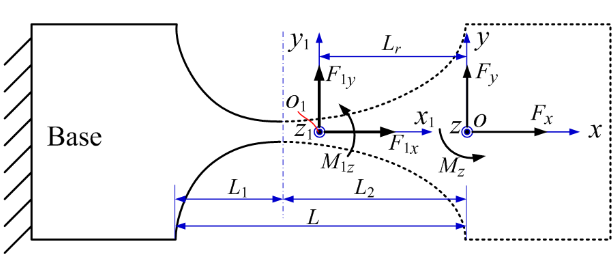

FIG. 4. The schematic of the NSFH under external unit forces.

respectively. For comparing the two hybrid NSFHs with the right-circular flexure hinges (RCFHs) and elliptical flexure hinges (EPFHs), the dependences of the planar compliances to variables L and c are also revealed. The radius of the RCFHs is set as $R_c = c/2 + L^2/(8c)$, while the major axis and minor axis of the EPFHs are set as $R_a = L/2$ and $R_b = c$, respectively. The resulted relationships of these four different hinges are shown in Fig. 5. Similarly, for investigating the influences of asymmetric ratio λ on the planar compliances, variables t, b, c, and L are chosen to be 1 mm, 10 mm, 5 mm, and 15 mm, respectively, while ratio λ ranges from 1/3 to 1, the acquired relationships are shown in Fig. 6.

From the relationships shown in Fig. 5, the planar compliances of the two hybrid NSFHs present increasing trends with the increase of length L, while the variation sensitivities of the compliances to variable L will slightly increase with the increasing L, except $\delta y/F_y$ has obvious increase. Moreover, parameter c has little influences on the planar compliances of the CNSFHs, but the planar compliances of the ENSFHs will slightly decrease with increasing c. The influences of parameters L and c on the planar compliances of the CNSFHs are more than the ENSFHs, while the variation sensitivities of the planar compliances to the length L are obviously stronger than the depth c. It shows that L can more strongly influence the performances of the proposed hybrid NSFHs.

In view of the NSFHs have trade-off relationships between the motion ranges and motion accuracies, so the comprehensive discussions should be made on the above two criteria, while the symmetric RCFHs and EPFHs are fairly compared with the proposed NSFHs. As shown in Fig. 5, all the compliances of the RCFHs and EPFHs are close to these of the ENSFHs except $\delta x/F_x$ and $\delta\theta_z/M_z$ of the EPFHs, and similar changing trends can be observed in above compliances. However, both $\delta x/F_x$ and $\delta\theta_z/M_z$ of the EPFHs more strongly decrease with increasing c than other compared hinges, as shown in Figs. 5(a) and 5(d). Additionally, the planar compliances of the RCFHs and EPFHs are less than these of the CNSFHs in most situations. In conclusion, $\delta y/F_y$ and $\delta y/M_z$ of the ENSFHs are slightly more than these of the EPFHs and RCFHs, while $\delta x/F_x$ and $\delta\theta_z/M_z$ of the ENSFHs are very close to these of the RCFHs. However, $\delta x/F_x$ and $\delta\theta_z/M_z$ of the CNSFHs more strongly decrease with increasing c than other hinges whose planar compliances have little dependences with the variable c.

As shown in Fig. 6, the dominant compliances also depend largely on the asymmetric ratio λ. Except $\delta x/F_x$ and $\delta\theta_z/M_z$ of the ENSFHs, all compliances of the two hybrid NSFHs will gradually decrease with increasing λ, while the variation sensitivities of these compliances to λ will decrease with the increase of λ. However, the two excepted compliances above

TABLE III. Comparison of precision factors between FEA results (denoted by F) and the FBMM results (denoted by A).

	$e_{x1}/F_x(\times10^{-10}\,\mathrm{m/N})$			$e_{y1}/F_y(\times10^{-7}\,\mathrm{m/N})$			$e_{y1}/M_z(\times10^{-6}\,1/\mathrm{N})$			$e_{\theta 1}/M_z(\times10^{-3}\,\mathrm{rad/m\,N})$		
	A	F	*e* (%)	A	F	*e* (%)	A	F	*e* (%)	A	F	*e* (%)
1	9.96	10.7	6.9	1.21	1.32	8.3	4.62	5.01	7.1	4.31	4.64	7.1
2	8.58	9.29	7.6	0.794	0.886	10	3.03	3.37	10.1	2.34	2.59	9.6
3	13.5	14.2	5.0	1.84	1.90	4.7	7.74	7.94	2.5	5.61	5.88	4.6

are nearly proportional to λ, whose variation sensitivities to ratio λ basically keep unchanged. For compliance $\delta\theta_z/M_z$, as shown in Figs. 5(d) and 6(d), the maximum value is multiple of the minimum one, this means that the hybrid NSFHs can provide a wider range of compliances and expand their applications with the suitable dimensional parameters.

B. Motion accuracy analysis and comparison

In view of the RCFHs and EPFHs are extensively applied in many fields, thus the motion accuracies should be fairly compared with the two hybrid NSFHs by the proposed NDPFs. For fair comparisons, variables t, b, and λ are, respectively, chosen to be 10 mm, 1 mm, and 0.5, while variables L and c range from 10 mm to 20 mm and 3 mm to 8 mm, respectively, then the related results are shown in Fig. 7. Similarly, influences of the asymmetric ratio λ on the precision factors of these four hinges are also investigated. Parameters L and c are chosen to be 15 mm and 5 mm, while variable λ ranges from 1/3 to 1, the relationships of the NDPFs in terms of variable λ are obtained and shown in Fig. 8.

As shown in Fig. 7, most NDPFs of the two hybrid NSFHs are less than these of the EPFHs and RCFHs, namely, the rotary centers of the hybrid NSFHs have less drifts under same motion ranges than other two hinges. As shown in Fig. 7(a), parameters L and c have little influences on β_1 of the RCFH and EPFH, while β_1 of the two hybrid NSFHs are slightly affected by variable L and c. As shown in Figs. 7(b) and 7(c), β_2 and β_3 of the ENSFHs are less than other three hinges, whose variation sensitivity to L and c is also less than other hinges. In additional, β_2 and β_3 of the CNSFHs are partly larger than these of the RCFH and EPFH when $c > 6$ mm and

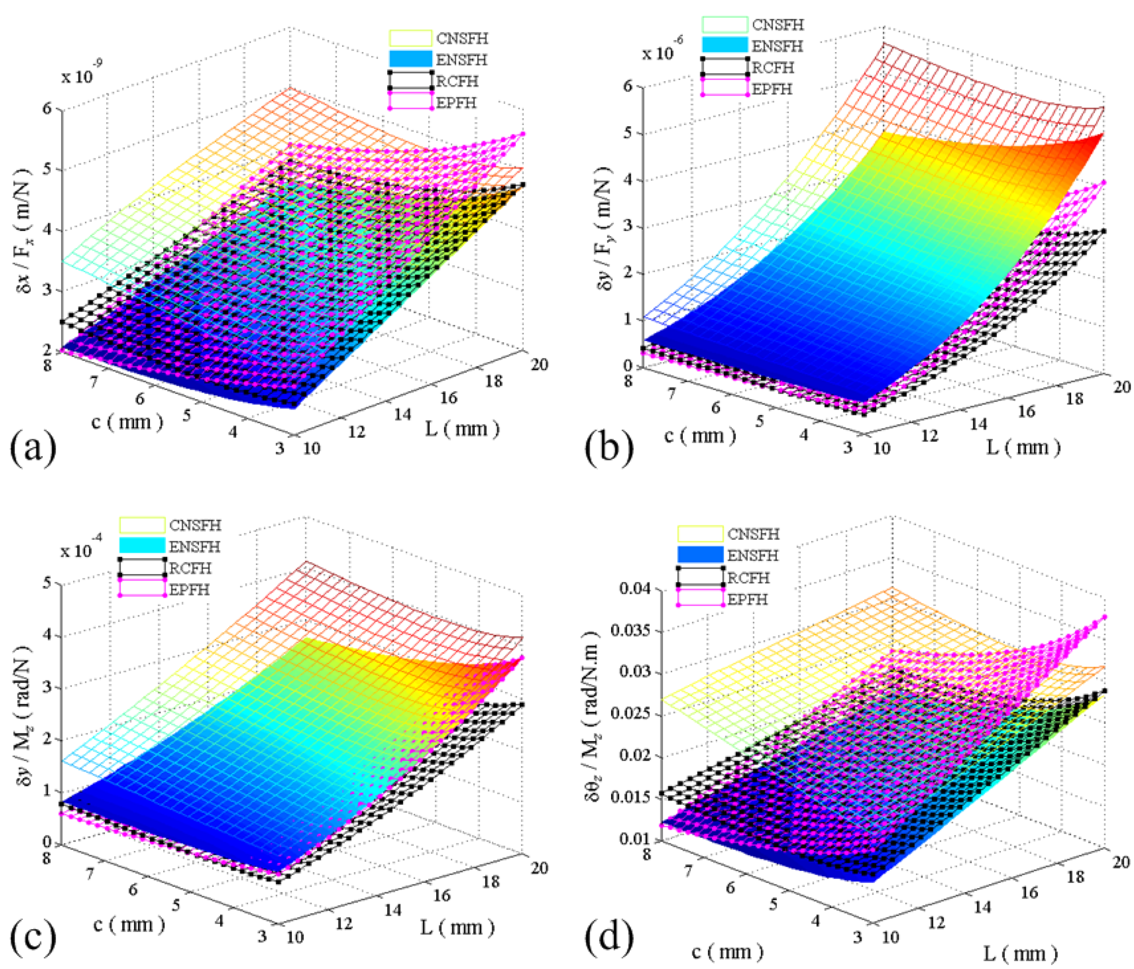

FIG. 5. Compliances of the hybrid NSFH with variable L and c. (a) $\delta x/F_x$, (b) $\delta y/F_y$, (c) $\delta y/M_z$, and (d) $\delta\theta_z/M_z$.

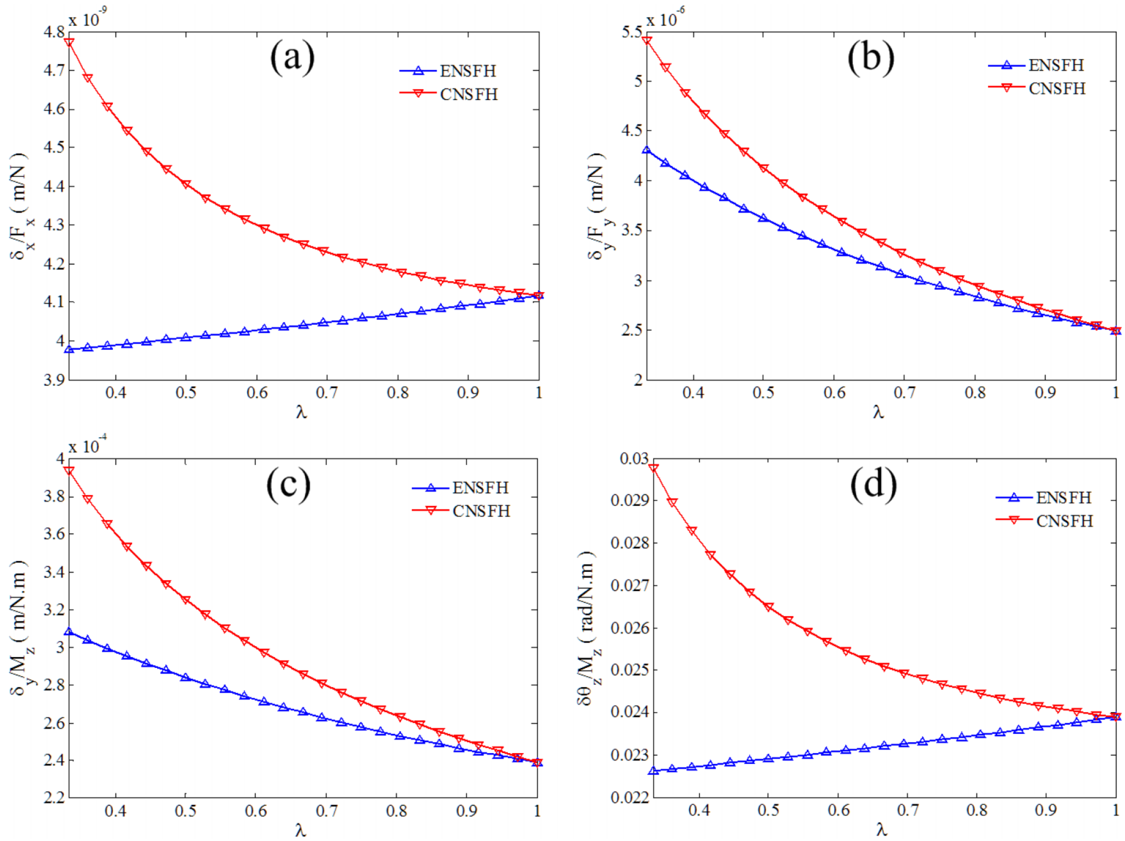

FIG. 6. Compliances of the hybrid NSFH with variable λ. (a) $\delta x/F_x$, (b) $\delta y/F_y$, (c) $\delta y/M_z$, and (d) $\delta\theta_z/M_z$.

L < 14 mm. Obviously, β_2 and β_3 of the CNSFHs are close to these of the RCFHs, but the ENSFHs are superior to other hinges. In view of the planar rotation of the rotary centers cannot directly contribute to the drift of the rotary centers, thus the present study will pay few attention on the related investigation.

As shown in Fig. 8, the motion accuracies $\boldsymbol{\beta}$ of the two hybrid NSFHs will increase with increasing variable λ except β_2 and β_3 of the CNSFHs, which have nonlinear relationships with ratio λ. The motion accuracies of the ENSFHs are completely less than these of the CNSFHs, and it indicates the ENSFHs have better motion precisions than the CNSFHs. Additionally, it is worth noting that β_2 and β_3 of the CNSFHs will be more than these of the symmetric hinges (λ = 1) when the ratio λ < 0.5. As shown in Figs. 5 and 7, the ENSFHs can exchange better motion accuracies than the RCFHs and EPFHs with the roughly same motion ranges. Although the CNSFHs can provide larger motion ranges than the ENSFHs, whose motion precisions are worse than the ENSFHs.

V. EXPERIMENT TESTS AND DISCUSSIONS

To verify performances of the two hybrid NSFHs, experimental tests are conducted on three prototypes of flexure hinges, namely, the ENSFH, CNSFH, and RCFH, which are monolithically fabricated by the wire electrical discharge machining method. For more fair comparison, same dimensional parameters and material properties are employed for the three prototypes of flexure hinges. The dimensional parameters are chosen as shown in Table I, and chosen material is spring steel 65Mn with the elastic modulus E = 2×10^{11} Pa and the Poisson's ratio μ = 0.288. As the photograph of experiment setup shown in Fig. 9, the equivalent compound loads

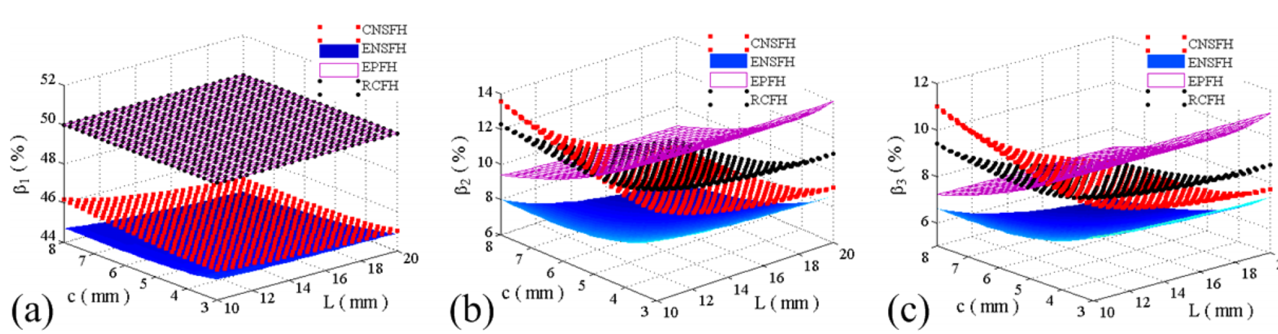

FIG. 7. Motion accuracy comparisons of the two hybrid NSFHs, RCFHs, and EPFHs with variable L and c. (a) β_1, (b) β_2, and (c) β_3.

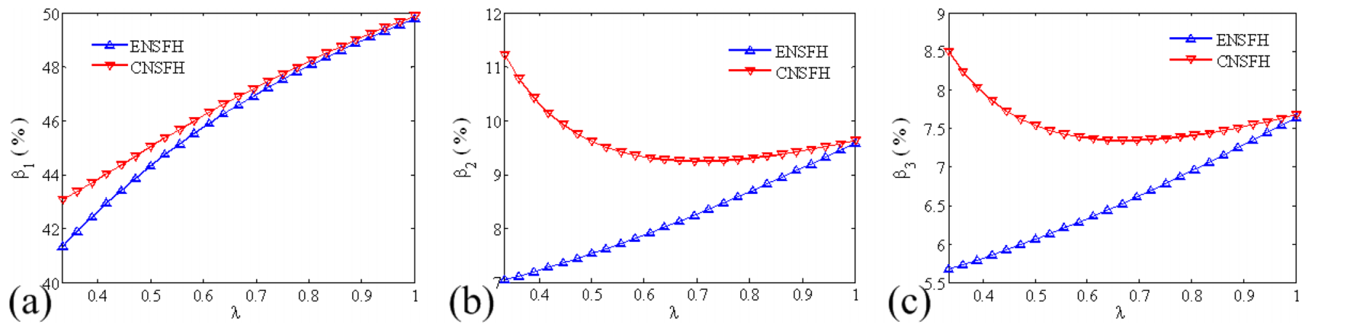

FIG. 8. Motion accuracies of the hybrid NSFHs with variable λ. (a) β_1, (b) β_2, and (c) β_3.

F involving the moments around the z-axis and push forces in the y direction are exerted on the free ends of flexure hinges, which can be measured by a force gauge. The output displacements of the point o are also measured by a capacity transducer (Micro-sense II 5300). All the experimental tests will be conducted on a vibration-isolated air-bearing platform (Newport RS4000) for reducing the adverse disturbances from external environment.

To verify the accuracy of the established FBMM model, the displacements under different external loads are experimentally measured, as shown in Fig. 10. The experimental results are fitted to obtain the compliances of tested hinges based on the least square method (LSM), and the corresponding fitted residuals are also obtained. The compliances are finally compared with the analytical and FEA results, as presented in Table IV.

As shown in Fig. 10, the experimental results show that there are perfect linear relationships between the external forces and output displacements of these three flexure hinges, and the experimental compliances (denoted by E) of the RCFH, CNSFH, and ENSFH are 1.331 μm/N, 2.193 μm/N, and 1.875 μm/N, respectively. With same dimensional parameters, the compliances of the hybrid NSFHs are more than these of the RCFH; namely, the two hybrid NSFHs can obtain larger motion ranges. As shown in Table IV, the relative errors between the FEA and analytical results are small, but the maximum deviations of experimental results are about 12%, which are caused by two main factors: (a) the geometric errors induced by the manufacture imperfect of the hinges and the systematic errors of the experimental processes and (b) the uncertain deviations of the chosen material properties between the experimental and theoretical processes. However, all experimental results fine match with the theoretical and FEA results, which can well demonstrate the accuracies of the established FBMM models of the proposed hybrid NSFH.

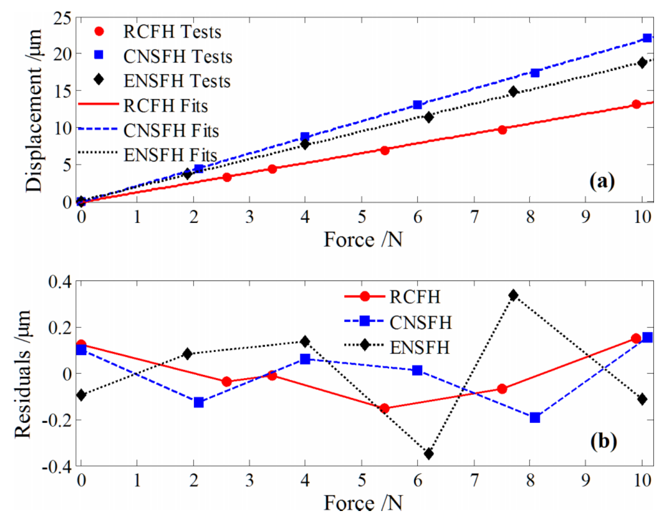

FIG. 10. Analysis of experimental results of different flexure hinges. (a) Experimental tests and fits and (b) the fitted residuals.

TABLE IV. Comparisons of experiment, FEA, and analytical results.

	RCFH (μ m/N)	CNSFH (μ m/N)	ENSFH (μ m/N)
A	1.543	2.463	2.019
F	1.548	2.449	2.021
E	1.331	2.193	1.875

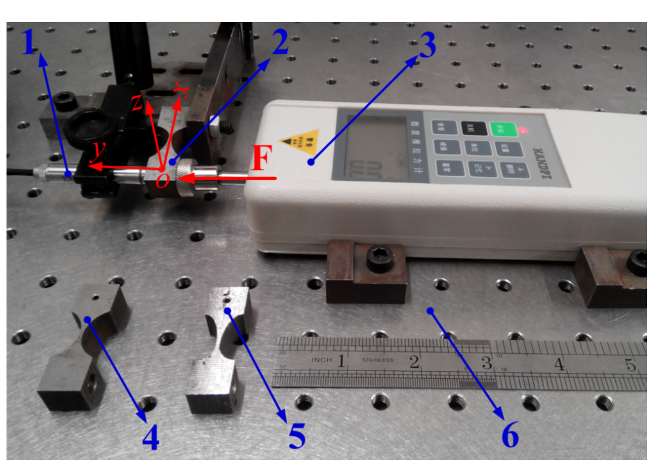

FIG. 9. The experimental setups (1. the sensor probe; 2. the ENSFH; 3. the force gauge; 4. the RCFH; 5. the CNSFH; and 6. the vibration-isolation air-bearing platform).

VI. CONCLUSIONS

In this paper, a novel type of non-symmetrical flexure hinges (NSFHs) with transversely asymmetric structures is developed to improve motion accuracies, whose compliance matrixes are analytically investigated by the FBMM method. The motion accuracies of two proposed hybrid NSFHs are characterized and compared with symmetric flexure hinges through introducing the NDPFs. Influences of the dimensional parameters on the compliances and motion accuracies of the two hybrid NSFHs are well revealed based on built FBMM model. This paper finally summarizes several main conclusions on the present studies as follows.

(a) Comparing with the FEA results, the maximum relative error of the analytical results is less than 5%, this indicates the established FBMM model, and derived maximum stress formula of the proposed NSFHs is effective.
(b) For the motion ranges and motion precision of the two hybrid NSFHs, the ENSFHs have better motion precisions than the symmetric hinges under roughly same motion ranges, but the CNSFH has larger motion ranges than the symmetric hinges under approximately equal motion precisions.
(c) Linear relationships can be observed between the external loads and output displacements in all experimental tests. The experimental and analytical results demonstrate the hybrid NSFHs have more excellent performances than the symmetric hinges.

ACKNOWLEDGMENTS

The authors are grateful to the financial support from the National Natural Science Foundation of China (NSFC) (Nos. 51175221, 51305162, and 51475208).

[1]W. Gao, T. Araki, S. Kiyono, Y. Okazaki, and M. Yamanaka, Precis. Eng. **27**(3), 289–298 (2003).
[2]Z. Zhu, X. Zhou, Q. Liu, and S. Zhao, J. Mech. Sci. Technol. **25**(12), 3141–3149 (2011).
[3]M. N. M. Zubir, B. Shirinzadeh, and Y. Tian, Sens. Actuators, A **150**(2), 257–266 (2009).
[4]Y. Li and Q. Xu, IEEE Trans. Autom. Sci. Eng. **8**(2), 265–279 (2011).
[5]Y. Li, J. Huang, and H. Tang, IEEE Trans. Autom. Sci. Eng. **9**(3), 538–553 (2012).
[6]Y. Yong, S. Moheimani, B. Kenton, and K. Leang, Rev. Sci. Instrum. **83**(12), 121101–121122 (2012).
[7]N. Lobontiu and M. Cullin, Precis. Eng. **37**, 542 (2013).
[8]N. Lobontiu, M. Cullin, M. Ali, and J. M. Brock, Rev. Sci. Instrum. **82**, 105116 (2011).
[9]N. Lobontiu and J. S. Paine, J. Mech. Des. **124**, 479 (2002).
[10]N. Lobontiu, J. S. Paine, E. Garcia, and M. Goldfarb, J. Mech. Des. **123**, 346 (2001).
[11]N. Lobontiu, J. S. Paine, E. Garcia, and M. Goldfarb, Mech. Mach. Theory **37**(5), 477–498 (2002).
[12]N. Lobontiu, J. S. Paine, E. O'Malley, and M. Samuelson, Precis. Eng. **26**(2), 183–192 (2002).
[13]G. M. Chen, X. D. Shao, and X. B. Huang, Rev. Sci. Instrum. **79**(9), 095103 (2008).
[14]G. M. Chen, X. Y. Liu, and Y. L. Du, J. Mech. Des. **133**(8), 081002 (2011).
[15]G. M. Chen, X. Y. Liu, H. W. Gao, and J. Y. Jia, Rev. Sci. Instrum. **80**(5), 055106 (2009).
[16]Y. Tian, B. Shirinzadeh, D. Zhang, and Y. Zhong, Precis. Eng. **34**(1), 92–100 (2010).
[17]Y. Tian, B. Shirinzadeh, and D. Zhang, Precis. Eng. **34**(3), 408–418 (2010).
[18]Q. Li, C. Pan, and X. Xu, Precis. Eng. **37**(1), 135–145 (2013).
[19]C. Gui-Min, J. Jian-Yuan, and L. Zhi-Wu, *presented at the Proceedings of IEEE Networking, Sensing and Control* (IEEE, 2005), pp. 700-704.
[20]G. M. Chen, J. Y. Jia, and Z. W. Li, *presented at the IEEE International Conference on Automation Science and Engineering* (IEEE, 2005), pp. 249-253.
[21]R. Lin, X. Zhang, X. Long, and S. Fatikow, Rev. Sci. Instrum. **84**(8), 085004 (2013).
[22]R. Q. Wang, X. Q. Zhou, and Z. W. Zhu, Rev. Sci. Instrum. **84**(9), 095008 (2013).
[23]Z. ZhiWei, Z. XiaoQin, W. RongQi, and L. Qiang, Sci. China: Technol. Sci. **58**(1), 56–63 (2015).
[24]Y. Koseki, T. Tanikawa, N. Koyachi, and T. Arai, *presented at the Proceedings of IEEE/RSJ International Conference on Intelligent Robots and Systems* (IEEE, 2000), p. 786.
[25]R. E. Peterson and R. Plunkett, J. Appl. Mech. **42**, 248 (1975).
[26]H. Lipkin and T. Patterson, *presented at the Proceedings of IEEE International Conference on Robotics and Automation* (IEEE, 1992), pp. 1251-1256.